RSC Advances

ROYAL SOCIETY OF CHEMISTRY

www.rsc.org/advances

AgAl alloy electrode for efficient perovskite solar cells

Yudan Luo[1], Xiaohong Chen[1,*], Chenxi Zhang[1], Junjie Li[1,3], Jianhua Shi[2], Zhuo Sun[1], Zhongchang Wang[3], Sumei Huang[1,*]

[1]Engineering Research Center for Nanophotonics & Advanced Instrument, Ministry of Education, Department of Physics, East China Normal University, North Zhongshan Rd. 3663, Shanghai 200062, P. R. China

[2]New Energy Technology Center, Shanghai Institute of Microsystem and Information Technology, 865 Chang Ning Road, Shanghai 200050, P. R. China

[3]Advanced Institute for Materials Research, Tohoku University, 2-1-1 Katahira, Aoba-ku, Sendai 980-8577, Japan

ABSTRACT

We report efficient mixed halide perovskite solar cells using thermally evaporated Ag or AgAl alloy layers as back electrodes. The properties of AgAl alloy and Ag films deposited on a hole-transport material layer for use in $CH_3NH_3PbI_{3-x}Cl_x$ solar cells were investigated. The influence of the distance between the metal source and the sample on the performance of solar cells was determined. The cell with an Ag layer deposited at a distance of 20 cm displayed a power conversion efficiency (PCE) of 5.49 %. When the Ag layer was deposited at a distance of 30 cm, the resulted device achieved a 46.8 % enhancement in PCE compared to the cell with the Ag

*Corresponding author: Fax: +86 21 62234321. E-mail address: smhuang@phy.ecnu.edu.cn (Sumei Huang); xhchen@phy.ecnu.edu.cn (Xiaohong Chen)

prepared at 20 cm. Furthermore, the AgAl alloy based perovskite solar cell accomplished a 37.3 % enhancement in PCE compared to the optimized Ag electrode. The fabricated AgAl alloy perovskite cells show a fill factor of 59.6 %, open-circuit voltage of 0.88 V, short‐circuit current density of 21.11 mA cm^{-2}, yielding an overall efficiency of 11.07%. The AgAl alloy layer exhibited high optical reflectivity and good adhesion on hole - transport material layer compared to a layer of Ag. The PCE enhancement mechanisms are discussed. Our work has demonstrated that AgAl is a promising back electrode material for high-efficiency perovskite solar cells.

KEYWORDS: mixed halide perovskite, solar cell, back electrode, metal alloy, interface, photovoltaics

1. INTRODUCTION

Perovskite solar cells (PSCs) have recently attracted a great deal of attention because of their excellent photovoltaic performance and facile and cheap fabrication processes. Since the introduction of $CH_3NH_3PbX_3$ (X = Br, I) by Miyasaka et al. as a sensitizer in an electrolyte based dye-sensitized solar cell structure, which marked the starting point of perovskite based photovoltaics[1, 2]. PSCs based on methylammonium lead halides have shown remarkable progress in terms of their power conversion efficiencies (PCEs). These solar cells utilizing a mesoporous scaffold, such as titania or alumina, the methylammonium lead halide perovskite light absorber, an organic hole - transport material (HTM), typically spiro-OMeTAD(2,2',7,7'-tetrakis-(N,N-di-p-methoxyphenylamine)-9,9'-bifluorene), and a gold back electrode have achieved a PCE of >10%.[3, 4] TiO_2/spiro-OMeTAD is the most successful couple owing to their good optical transparency, perfect band alignment with respect to methylammonium lead iodide ($MAPbI_3$). The PCEs were improved to 15% by using a two-step sequential deposition technique, involving spin-coating of a PbI_2 followed by exposure to a solution of MAI to form $MAPbI_3$, or a dual-source vapor deposition technique to fabricate a planar heterojunction solar cell[5-7]. Recently, a planar structured perovskite solar cell using an ITO electrode modified with polyethyleneimine ethoxylated, a yttrium-doped TiO_2 layer, the mixed halide perovskite $MAPbI_{3-x}Cl_x$ absorber and spiro-OMeTAD achieved a PCE of 19.3%[8].

In order to maximize the attainable open circuit voltage (Voc), low chemical potential, namely, high work function noble metals, such as gold[5, 9] and silver[6] are generally used as back electrode for PSCs. Thermal evaporation of gold is a very expensive and unproductive process because only a minute portion of gold is eventually deposited onto the devices. The high cost of the Au electrode limits its future application in PSCs. Furthermore, growth of metal electrode requires a high-vacuum and high-temperature evaporation technique, however, perovskite organic lead iodide is unstable at temperatures significantly below 300 °C[10, 11]. The $MAPbI_3$ perovskite was found to decompose at 140 °C, leaving behind the inorganic PbI_2, which is detrimental to the photovoltaic performance of the device. Therefore, avoiding the thermal effect from the reactive hot metal atoms or the heater on the perovskite absorber may be a key consideration in designing the evaporator or choosing suitable metal sources toward the production of efficient and low-cost perovskite solar cells. Moreover, PSC devices have one or more organic layers contained within layers of metals such as Au and Ag. Contact resistance in ohmic contact is one of the important design parameters that are necessarily controlled to ensure efficient and reliable charge transport and extraction process in solar cells. The interfacial adhesion between the metal electrode and the organic film crucially determines the device performance and stability. However, with so much focus on perovskite film processing[3-8], absorber layer surface coverage[12], crystal quality optimization[13] and alternative hole transport materials owing to the high cost of spiro-OMeTAD[14,15] as well as bandgap tuning[16], there are only few reports where

metal electrode processes and physical properties are studied [17, 18].

In this study, we demonstrate for the first time thermal evaporation processing of AgAl alloy as back electrodes for efficient mixed halide perovskite solar cells. The properties of AgAl alloy or Ag layer deposited on a spiro-OMeTAD HTM layer for use in high-efficiency PSCs were investigated. The dependence of the performance of $MAPbI_{3-x}Cl_x$ solar cells on the distance between the metal source and the sample during the thermal evaporation process was determined. The cell with an Ag layer deposited at a distance of 20 cm displayed a PCE of 5.49 %. With the Ag layer deposited at a distance of 30 cm, the resulted device achieved a 46.8 % enhancement in PCE compared to the cell with the Ag prepared at 20 cm. The PCE enhancement can be associated with the decreased agglomeration of the Ag film and the improved adhesion between the Ag and the HTM. Moreover, the output PCE of the perovskite solar cell was further significantly enhanced when the AgAl alloy electrode grown at 30 cm was employed. The AgAl alloy based cell accomplished a 37.3 % enhancement in PCE compared to the optimized Ag electrode. This result can be attributed to the dense, compact, smooth and homogeneous properties of AgAl and its good adhesion to the spiro-OMeTAD HTM layer. Our work suggests that AgAl represents a promising back electrode material for high-efficiency perovskite solar cells.

2. EXPERIMENTAL SECTION

2.1 Preparation of the PSCs

Fluorine-doped tin dioxide SnO_2 (FTO)-coated glass sheets (< 15 Ω/square, Nippon Sheet Glass Co., Ltd., Japan, or ultra thin FTO, Shanghai Materwin New Maters Co., Ltd., China) were etched with zinc powders and HCl (2 M) to obtain the required electrode patterns. The sheets were then cleaned by sonication in glass detergent (Hui Jie washing Ltd., Shenzhen), de-ionized water, acetone and methanol and finally subsequently dried in a vacuum oven. A 30 - 50 nm thick TiO_2 compact layer was then deposited on the cleaned FTO substrates by a sol-gel method. To prepare the TiO_2 compact film precursor solution, titanium isopropoxide (369 μl) was diluted in isopropanol (2.53 ml) at 0.46 M. In addition, a 2M HCl solution (35 μl) was separately diluted down with isopropanol (2.53 ml) to achieve a 0.026M concentration. Then, the acid-containing solution was added dropwise to the titanium precursor solution under heavy stirring. The resulted solution was filtered with a polytetrafluoroethylene (PTFE) filter with 0.2 μm pore size before use. The etched FTO substrates were coated with a compact layer by spin coating the TiO_2 blocking film precursor solution at 2,000 r.p.m. for 60 s, and consequently heating at 500 °C for 30 min. After cooling down to the room temperature (~ 25 °C), the sample was treated in a 40 mM $TiCl_4$ aqueous solution at 70°C for 30 min in order to improve the adhesion and mechanical strength of the TiO_2 layer to the FTO layer[19]. At last, the sample was rinsed with de-ionized water and anhydrous alcohol, and heating at 500 °C for 30 min.

0.5 μm-thick mesoporous TiO_2 layer was deposited by spin-coating TiO_2 paste (Dyesol

18NR-T) diluted in anhydrous ethanol at 1 : 3.5 by weight at 2000 r.p.m for 50 s. The layers were then sintered in air at 500 ºC for 30 minutes. After cooling down to the room temperature, the samples were also treated using the $TiCl_4$ aqueous solution at 70°C for 30 min and dried at 500 °C for 30 min. After cooling down to room temperature, the perovskite was deposited by spin-coating from a *N*,*N*-Dimethylformamide (DMF solution of methylammonium iodide and $PbCl_2$ (3:1 molar ratio), as described elsewhere[3], which formed the perovskite after heating to 100 °C for 45 min in an oven.

The hole-transport layer was deposited by spin-coating a spiro-OMeTAD solution at 4,000 r.p.m. for 30 s. The spin-coating solution was prepared by dissolving 0.0723 g spiro-MeOTAD, 28.8 µl 4-tert-butylpyridine, 17.5 µl of a stock solution of 0.520 g ml^{-1} lithium bis(trifluoromethylsulphonyl)imide in acetonitrile and 29 µl of a stock solution of 0.300 g ml^{-1} tris(2-(1H-pyrazol-1-yl)-4-tert-butylpyridine)cobalt(III) bis(trifluoromethylsulphonyl)imide in acetonitrile in 1 ml chlorobenzene. Finally, about 100 nm-thick Ag or AgAl alloy was thermally evaporated on top of the device to form the back contact at different distances (20 cm and 30 cm) between the metal source and the substrate using a home-made thermal evaporation system. Pure (99.99%) Ag or AgAl alloy (Al: 3 wt.%) wire was used as the metal source for the thermal evaporation. The base pressure of the deposition chamber was about 1×10^{-4} Pa. The deposition rate and thickness of metallic layers were monitored with quartz crystal monitors, and the active device area is 0.09 cm^2. The obtained PSC solar cell

with an Ag back electrode deposited at a distance of 20 cm was referred as PSC-Ag1, and cells with Ag and AgAl electrodes deposited at a distance of 30 cm are referred as PSC-Ag2 and PSC-AgAl, respectively.

2.2 Characterization of samples

Cross-sectional measurements: cross-section specimen for transmission electron microscopy (TEM) was fabricated by focused ion beam (FIB) technique and using the Hitachi FB2200 FIB system. After the FIB, the TEM specimens were cleaned by Ar ion-beam thinning with an accelerating gun voltage of 0.5-1.0 kV to reduce electron radiation damage. The TEM measurements were performed using an acceleration voltage of 200 kV on a JEOL-2010F (JEOL Co. Ltd) transmission electron microscope equipped with an energy dispersive X-ray spectrometer (EDX). TEM in combination with EDX provides precise elemental maps by means of locally recording the spectrum of emitted X-rays. It should be noted that the resulting elemental maps yield only a relative concentration distribution.

X-ray diffraction 2θ scans were obtained from samples of perovskites deposited on the compact /porous TiO_2 -coated FTO-coated glass using an X-ray diffractometer (XRD, Bruker D8 Davinci instrument, Cu-Kα: λ = 0.15406 nm). And the morphologies of the deposited Ag and AgAl alloy layers were characterized by field emission scanning electron microscope (FESEM, Hitachi S4800). Element analysis of the AgAl alloy layer was measured by an EDX attached to the above FESEM. The

thickness of the layers were measured by a profilometer (Dektak 6M). Photocurrent density–voltage (*J-V*) measurements were performed using an AM 1.5 solar simulator equipped with a 1000 W Xenon lamp (Model No. 91192, Oriel, USA). The solar simulator was calibrated by using a standard Silicon cell (Newport, USA). The light intensity was 100 mW cm^{-2} on the surface of the test cell. *J-V* curves were measured using a computer-controlled digital source meter (Keithley 2440) with the forward direction. During device characterization, a metal aperture mask with an opening of about 0.09 cm^2 was used.

3. RESULTS AND DISCUSSION

J-V characteristics of perovskite solar cells with different metal electrodes under a light intensity of 100 mW cm^{-2} are presented in Fig. 1. The mesoporous TiO_2 film was infiltrated with the $CH_3NH_3PbI_{3-x}Cl_x$ perovskite nanocrystals using the above-mentioned single step procedure. This active layer has a thickness of around 600 nm. The thickness of metallic layer is 100 nm. Although $CH_3NH_3PbI_3$ has been widely applied on nanostructured TiO_2 electrodes, there are very few reports about $CH_3NH_3PbI_{3-x}Cl_x$ in a mesoporous nanostructure[3, 20]. Our $CH_3NH_3PbI_{3-x}Cl_x$ solar cell has a similar architecture to the mesoporous $CH_3NH_3PbI_3$ device reported in[5], except that a thinner mesoporous TiO_2 layer (about 300 nm in thickness) and an Au electrode were used in the latter. Device parameters including PCE (η), open-circuit voltage (V_{OC}), short‐circuit current density (J_{sc}) and fill factor (FF) are summarized in Table 1. As shown from Figure 1 and Table 1, the PSC (referred as PSC-Ag1) with an Ag

layer deposited at a distance of 20 cm displays a J_{sc} of 11.68 mA cm^{-2}, FF of 56.0 %, V_{oc} of 0.84 V and η of 5.49 %. The efficiency was a little poorer than that (8.6 %) reported for the solution processed $CH_3NH_3PbI_{3-x}Cl_x$ planar heterojunction solar cell in Ref[6]. However, when the distance between the metal source and the substrate changed from 20 cm to 30 cm, even using the same Ag metal source, the formed PSC achieved much better performance. The solar cell (PSC-Ag2) with an Ag layer deposited at a distance of 30 cm displays an obviously improved J_{sc} of 15.83 mA cm^{-2}, V_{oc} of 0.88 V, FF of 57.9 % and η of 8.06 %. The device achieved very comparable photovoltaic paramters to those attained for the solution processed $CH_3NH_3PbI_{3-x}Cl_x$ planar cell in Ref [6]. Surprisingly, when the AgAl alloy was used as the source, the photovoltaic performance was furthermore improved. The solar cell (PSC-AgAl) shows a J_{sc} of 21.11 mA cm^{-2}, V_{oc} of 0.88 V, *FF* of 59.6 %, and thus, the highest η of 11.07 %. With improved J_{sc} and FF values as well as the same high V_{oc}, the PCE of PSC-AgAl is increased by 37.3 % relative to PSC-Ag2 based on the same thick Ag layer deposited at 30 cm.

The improved photovoltaic performance might be attributed to the increased light absorption, the enhanced charge injection and/or charge collection efficiency because the PSC-AgAl hybrid solar cell exhibited better IPCE spectrum than the PSC-Ag2 cell as shown in Fig. 2. IPCE is often referred to as quantum efficiency, a collective measure of light harvesting, charge separation and charge collection efficiencies. Therefore, IPCE depends on both the absorption of light and the

collection of charges. As exhibited in Fig. 2, the PSC-AgAl possesses enhanced photo-response in comparison with the PSC-Ag2. The latter show a wide photo-response from visible to the near-infrared, with IPCE values around 60% at 400 – 600 nm, while the PSC-AgAl gives a noticeable improvement of the photocurrent from 450 to 800 nm. Moreover, the IPCE spectra of both cells are in good agreement with the optical reflectance curves of their metal back electrodes shown in Fig. 2. The evaporated AgAl layer exhibited higher optical reflectance than the deposited Ag layer in the 450 – 800 nm region. The reflective results correlated well with those reported in ref. 21. The lower IPCE efficiency of the PSC-Ag2 at long wavelength arose from inefficient charge extraction and/or light harvesting[22], resulting in the relative lower J_{sc} of solar cells shown in Fig. 1 and Table 1. The higher IPCE values of the PSC-AgAl can be associated with efficient charge extraction due to the reduced parasitic resistance at the metal and the HTM interface, which is described in the posterior section. Besides, from Fig. 2, the increased reflectance in the back contacts could enhance the light absorption in the solar cells. Therefore, to some extent, the high IPCE in the 450 – 800 nm region from the PSC-AgAl is probably due to the reflection effect at the alloy back contact.

Figure 3 compares the X-ray diffraction patterns of as-grown porous TiO_2 covered FTO slide and $CH_3NH_3PbI_{3-x}Cl_x$ deposited on the mesoporous TiO_2 film. Diffraction peaks are observed at approximately 14.2°, 20.0°, 28.5°, 31.9°, 35.0°, 40.6° and 43.2°, respectively, corresponding to the reflections from (110), (112), (220), (310), (312),

(224) and (314) crystal planes of the tetragonal perovskite structure, similar to the $CH_3NH_3PbI_3$ previously reported[23, 24].

To determine the functional components and their elemental composition in the device, we carried out TEM measurements in combination with EDX on the cross section of PSC-Ag1 (Figure 4). For this purpose, a thin TEM lamellae sample was prepared with the help of a focused ion beam. In the TEM image (the top left of Figure 4), distinct layers with different features and contrasts can be observed in the fabricated device. A compact and dense TiO_2 layer is on top of FTO, followed by a mesoporous layer. The elemental analysis showed that the Si, Sn, Ti, Pb, I and Ag distributions are agreement with the suggested cell structure. Furthermore, TEM–EDX showed that Pb and I are present throughout the mesoporous layer. Some Cl signal was also observed (not shown in the figure). Almost no oxidation was observed in the formed Ag electrode according to the Ag and O distributions from the EDX measurement. Moreover, Ag forms a continuous layer on HTM, and there is no diffuse interface between them. In addition, the cross-sectional high-resolution TEM image of mesoporous TiO_2 film infiltrated with $MAPbI_{3-x}Cl_x$ for Device PSC-Ag1 was shown in Fig. 5. The (101) lattice plane of Anatase TiO_2 and the (310) lattice plane of $MAPbI_{3-x}Cl_x$ are identified in the upper left and the lower right insets of Fig. 5(b), respectively. The results are consisted with the findings from the XRD measurements shown in Fig. 3.

It is well known that the metal/organic interface plays an essential role in determining the overall device performance of organic electronics, and diffusion and reaction between the metal electrode material and polymer have to be suppressed. While Au, Al and Ag are the most common electrode materials for organic photovoltaic (OPV) devices, the thermal evaporation process frequently alters the quality of the metal/organic interface[25-29], which essentially affects the overall device performance. It is found that the reactive hot metal atoms can lead to chemical interaction at the interface and diffusion into the organic layer[30, 31]. The chemical reaction at the metal/organic interface can also vary the contact properties, forming interfacial dipole barriers and defect states that pin the Fermi level[32, 33], and the metal ion diffusion into the organic layer has a detrimental effect on the performance and cause substantial leakage current[34, 35]. In contrast, no clear Ag ion diffusion into the organic HTM layer was observed in our fabricated devices even at the evaporation distance of 20 cm by our elemental mapping characterization shown in Fig. 4.

In order to understand underlying mechanisms for the lowest PCE from the PSC-Ag1, the series resistance (R_S) and shunt resistance (R_{SH}) were estimated from the J–V characteristics shown in Fig. 1. The R_S and R_{SH} values from these devices are summarized in Table 1. As shown in Table 1, it is observed that all three devices show quite similar R_{SH} values, but their R_S resistances are significantly different. The increase of the distance between the metal source and the substrate leads to an obvious reduction in R_S. PSC-Ag2 shows a 49.4 % reduction in R_s compared to the

case of PSC-Ag1. Additionally, the introduction of AgAl alloy layer induces a 63.2% reduction in R_S of PSC-AgAl compared to that of PSC-Ag1, which in turn significantly increases the total enhancement in the PCE of the former.

Commonly, the shunt resistance (R_{SH}) is due to p-n junction non-idealities and impurities near the junction, which cause partial shorting of the junction, particularly near cell edges, but nevertheless the major contributors to the series resistance (R_S) are the bulk resistance of the semiconductor material (the active layer), the contact resistance at the semiconductor-metal interfaces and the resistance of the metal contacts[36, 37]. The R_{SH} must be higher to avoid current loss at the junction, dwindling the photocurrent and the fill factor of a cell, and hence the solar cell performance. In the case PSCs, it has been widely reported that the pinholes formed in the solution-processed $CH_3NH_3PbI_{3-x}Cl_x$ absorber films will result in direct contact of the p-type spiro-OMeTAD and the TiO_2 compact layer, leading to a shunting path that is probably partially responsible for the low fill factor and open-circuit voltage in devices[6, 12]. Contrarily to the R_{SH}, maintaining the R_S as low as possible is of paramount importance because large R_S will decrease J_{sc} , V_{oc}, *FF*, and consequently PCE[38, 39]. The low R_S is usually associated with efficient charge transport with negligible charge accumulation and recombination in device. In fact, the low R_S from a PSC is typically due to low bulk resistance of the high-quality perovskite layer, small electrode resistance and low contact resistance, indicating that high currents can flow through the cell at low applied voltages[40]. In our work, solar cells PSC-Ag1,

PSC-Ag2 and PSC-AgAl were deposited using the same conditions, except for the thermal evaporation process of the metal electrode. All three devices display similar V_{OC} and FF values. The V_{OC} and FF of the cell using the Ag layer deposited at 20 cm is 0.84 V and 56.0 %, respectively, only slightly lower than those of the cells using the Ag or AgAl film deposited at 30 cm. In addition, the R_{SH} resistance of PSC-Ag1 is quite similar to those of the other two cells, which suggests that the prefabricated absorber layer is kept intact after the metal thermal evaporation processing even at the small distance. In contrast, compared to the J_{sc} of 21.11 mA cm^{-2} for the cell using the AgAl, the J_{sc} value (11.68 mA cm^{-2}) found in the device using the Ag deposited at 20 cm is considerably low, which is responsible for the low conversion efficiency in the latter device. Since there is no significant difference in V_{oc}, *FF* and R_{SH} in comparison to the other two cells, we attribute the low J_{sc} and thus PCE in PSC-Ag1 mainly to its high series resistance. Indeed, the series resistance (R_S) at Voc for the PSC-Ag1 cell is 220.7 Ω, over 2.7 times higher than that of the AgAl backed cell. Moreover, no Pb or I ion diffusion into the HTM layer was detected in the cell with the Ag even deposited at the short distance of 20 cm as shown in Fig. 4, and this device achieved a FF of 56.0 % and η of 5.49 %, which also indicates that the absorber is able to endure the metal thermal evaporation processing conditions. The component ratio of the AgAl alloy layer deposited at a distance of 30 cm was determined by EDX shown in Fig. 6. The evaporated AgAl film contains 96.1 at.% Ag and 3.9 at.% Al. As a result, the resistivity of either Ag or AgAl alloy is very low. The bulk resistances of the metal electrodes are negligible. The absorber layers were made under the same conditions

and stood the following evaporation processing. Therefore, the significantly reduced R_S in the PSC-AgAl can be associated with a reduced parasitic resistance at the metal and the HTM interface.

In order to make a further research on underlying mechanisms for the lowest PCE from the PSC-Ag1, the morphological properties of the metal layer and the interface between the metal and the HTM are carefully examined and analyzed. Figure 7 shows a cross-sectional SEM picture of a PSC device with the Ag layer deposited at 20 cm. The device was made using the same conditions for the above device fabrication, except that thick Ag and active layers were prepared in order to clearly distinguish the various functional layers of the device through SEM. An about 1 μm-thick $CH_3NH_3PbI_{3-x}Cl_x$ sensitized film was formed on the compact TiO_2 layer. A ~200 nm Ag layer was thermally evaporated onto the HTM at a distance of 20 cm, forming the back contact of the device. The morphological structure of our mesoporous $CH_3NH_3PbI_{3-x}Cl_x$ active layer greatly resembles the case of the mesoporous $CH_3NH_3PbI_3$ reported in[5]. As is evident in Figure 7, the surface morphology of the formed Ag layer deposited at 20 cm is quite roughened. The Ag electrode is consisted of agglomerated particles (20 - 100 nm in size). Its adhesion to the HTM is bad because of the serious agglomeration. In addition, there are many voids between the Ag layer and the underlying HTM film.

In order to examine the physical properties of Ag and AgAl electrodes of

PSC-Ag2 and PSC-AgAl, HTM layers were spin-coated on FTO slides, and then, Ag and AgAl layers were thermal deposited on the formed HTM films at a distance of 30 cm, respectively, using the same conditions for the device fabrication, producing samples FTO/HTM/Ag and FTO/HTM/AgAl. Figures 8 and 9 show SEM images of the cross-sections and top surfaces of these two samples, respectively. Interfacial voids also presented between the Ag layer and the HTM film for the sample FTO/HTM/Ag while the AgAl alloy layer closely and perfectly covered the underlying HTM surface as shown in Figures 8 (a) and (b), respectively. Moreover, from the top surface images of the Ag and AgAl films shown in Figures 9 (a) - (d), the alloy layer shows flatter, smoother, more homogeneous and more compact morphology than the Ag film. The morphology of the formed AgAl film shows grains about 25 nm in diameter while the grain size of the Ag layer is about 15 - 30 nm, as shown in Figures 9 (b) and 9 (d), respectively. By comparing the morphological properties of the AgAl film deposited at 30 cm and Ag layers deposited at 20 cm and 30 cm shown in Figures 7 - 9, the AgAl alloy layer has the best adhesion to the HTM, and the Ag layer deposited at 30 cm takes the second place.

As a matter of fact, agglomeration behavior of evaporated Ag films suppressed by alloying with Al or Cu elements in small amounts was reported in the late 21st century[21, 41]. AgAl alloy layers were developed and widely used for GaN-based light-emitting diodes (LEDs) because of their high thermal stability, high reflectance in visible light and reasonable ohmic behaviors[21]. The Ohmic properties of Ag and

AgAl were comparatively investigated. It was found that Ag suffered from poor adhesion to *p*-GaN due to agglomeration during the annealing process, leading to deterioration in its electrical and optical properties, while the AgAl layer showed good adhesion properties compared to a layer of Ag on *p*-GaN. Moreover, Ag–Al alloy ohmic contacts were demonstrated to improve the thermal stability of Ag-based ohmic contacts[21]. Agglomeration suppression and thermal stability improvement of AgAl layer could be associated with the formation of very thin Al-oxide layers at the film surface and at the interface with the substrate[21, 42]. Our experimental results about Ag and AgAl alloy electrodes are consisted well with those reported in these previous works[21, 42]. As shown from Figures 5 - 7, stronger agglomeration was observed on the Ag surface of PSC-Ag1 due to the thermal effect with the evaporation at the small distance. When the distance is increased to 30 cm, the Ag size is three times smaller, and the agglomeration became slighter due to the less thermal effect during the thermal evaporation at the larger distance. Therefore, considering the same thick Ag layer for PSC-Ag1 and PSC-Ag2, the major contribution to the observed 49.4 % decrease in R_S of the latter, as shown in Table 1, may be related to the smaller contact resistance at the Ag/HTM interface. The lower R_S resistance results in the higher FF and J_{sc} values, thus, the improved PCE in PSC-Ag2 compared to PSC-Ag1. Device PSC-Ag1 shows the highest series resistance R_S value, which is largely due to severe formation of agglomeration and growth of holes during the thermal processing of the Ag layer. The highest R_S resistance induces the poorest performance of PSC-Ag1. In addition, the interfacial voids observed on the Ag surface for PSC-Ag2 or PSC-Ag1

disappeared on the AgAl alloy. No void or agglomeration was found in the AgAl film, which indicates that the AgAl layer is thermally stable, which results in the excellent adhesion on the HTM layer. This increased contact area further decreases the R_S resistance and increases the charge collection efficiency, which contributes to the highest FF, J_{sc} and thus best conversion efficiency of the resulting devices shown in Fig. 1 and Table 1. As a result, PSCs using AgAl alloy as back electrodes show better charge collection abilities and improved photovoltaic properties in contrast to the optimized device with Ag layer. The fabricated AgAl alloy perovskite cells exhibit an overall efficiency of 11.07%. This is the first report of the successful evaporation processing of AgAl alloy as back electrodes for efficient mixed halide perovskite solar cells as far as we know.

4. CONCLUSIONS

We reported efficient $CH_3NH_3PbI_{3-x}Cl_x$ solar cells using thermally evaporated AgAl alloy or Ag as back electrode. The influence of the distance between the metal source and the sample during the evaporation processing on the performance of solar cells was investigated. The cell with an Ag layer deposited at a distance of 20 cm exhibited J_{sc} of 11.68 mA cm^{-2}, FF of 56.0 %, V_{oc} of 0.84 V and corresponding PCE of 5.49 %. In contrast, the device with the Ag deposited at 30 cm displayed J_{sc} of 15.83 mA cm^{-2}, V_{oc} of 0.88 V, FF of 57.9 % and corresponding PCE of 8.06 %. This cell achieved a 46.8 % enhancement in PCE compared to the device with the Ag prepared at 20 cm. The PCE enhancement can be attributed to the decreased agglomeration of

the thermally evaporated Ag film and the improved adhesion between the Ag and the HTM. Moreover, the output PCE of the perovskite solar cell was further significantly enhanced when the AgAl alloy back electrode was employed. The alloy layer deposited at 30 cm possesses the densest, smoothest and most homogeneous surface morphology, therefore the best adhesion between the metal layer and the underlying HTM, and the smallest series resistance (R_S), resulting in a PCE high up to 11.07 %. High optical reflective properties of AgAl alloy also contributed to the performance improvement of the device. These results indicate that the AgAl alloy is a promising back electrode material and ohmic scheme for high efficiency perovskite solar cells.

ACKNOWLEDGEMENTS

This work was supported by the National Natural Science Foundation of China (Nos. 11274119 and 61275038) and the Large Instruments Open Foundation of East China Normal University.

REFERENCES

1. A. Kojima, K. Teshima, Y. Shirai and T. Miyasaka, *J. Am. Chem. Soc.*, 2009, **131**, 6050–6051.
2. J.-H. Im, C.-R. Lee, J.-W. Lee, S.-W. Park and N.-G. Park, *Nanoscale,* 2011, **3**, 4088–4093.
3. M. M. Lee, J. Teuscher, T. Miyasaka, T. N. Murakami and H. J. Snaith, *Science*, 2012, **338,** 643–647.
4. H.-S. Kim, C.-R. Lee, J.-H. Im, K.-B. Lee, T. Moehl, A. Marchioro, S.-J. Moon, R. Humphry-Baker, J.-H. Yum, J. E. Moser, M. Grätzel and N.-G. Park, *Sci. Rep.*, 2012, **2**, 591.
5. J. Burschka, N. Pellet, S-J. Moon, R. Humphry-Baker, P. Gao, M. K. Nazeeruddin and M. Grätzel, *Nature*, 2013, **499**, 316–320.
6. M. Liu, M. B. Johnston and H. J. Snaith, *Nature*, 2013, **501**, 395–398.
7. D. Liu and T. L. Kelly, *Nat. Photonics*, 2014, **8**, 133–138.
8. H. Zhou, Q. Chen, G. Li, S. Luo, T-B. Song, H-S. Duan, Z. Hong, J. You, Y. Liu, and Y. Yang, *Science*, 2014, **345,** 542–546.
9. H. Li, K. Fu, A. Hagfeldt, M. Gratzel, S. G. Mhaisalkar and A. C. Grimsdale, *Angew. Chem., Int. Ed*., 2014, **53**, 4085−4088.
10. T. Supasai, N. Rujisamphan, K. Ullrich, A. Chemseddine and Th. Dittrich, *Appl. Phys. Lett.*, 2013, **103**, 183906.
11. A. Dualeh, N. Tétreault, T. Moehl, P. Gao, M. K. Nazeeruddin and M. Grätzel, *Adv. Funct. Mater.,* 2014, **24**, 3250−3258.
12. G. H. Eperon, V. M. Burlakov, P. Docampo, A. Goriely and H. J. Snaith, *Adv. Funct. Mater.*, 2014, **24**, 151–157.
13. M. Xiao, F. Huang, W. Huang, Y. Dkhissi, Y. Zhu, J. Etheridge, A. Gray-Weale, U. Bach, Y.-B. Cheng and L. Spiccia, *Angew. Chem., Int. Ed*., 2014, **53**, 9898–9903.
14. L. Etgar, P. Gao, Z. Xue, Q. Peng, A. K. Chandiran, B. Liu, M. K. Nazeeruddin and M. Grätzel, *J. Am. Chem. Soc.*, 2012, **134**, 17396–17399.
15. A. Mei, X. Li, L. Liu, Z. Ku, T. Liu, Y. Rong, M. Xu, M. Hu, J. Chen , Y. Yang, M.

Gratzel and H. Han, *Science,* 2014, **345**, 295−298.

16. N. G. Park, *Mater. Today*, 2015, **18**, 65-72.
17. Q. Jiang, X. Sheng, B. Shi, X. Feng , T. Xu, *J. Phys. Chem.* 2014, **118**, 25878–25883.
18. F. Guo, H. Azimi, Y. Hou, T. Przybilla, H. Mengyao, C. Bronnbauer, S. Langner, E. Spiecker, K. Forberich and C. Brabec, *Nanoscale*, 2015, **7**, 1642–1649.
19. D. Zhang, X. Li, H. Li, S. Chen, Z. Sun, X. Yin, S. Huang, *Carbon*, 2011, **49**, 5382–5388.
20. S. Bretschneider, J. Weickert, J. Dorman and L. Schmidt-Mende, *APL Mater.*, 2014, **2**, 040701.
21. J.-Y. Kim, S.-I. Na, G.-Y. Ha, M.-K. Kwon, I.-K. Park, J.-H. Lim, and S.-J. Park, *Appl. Phys. Lett*., 2006, **88**, 043507.
22. F. Hao, C. C. Stoumpos, Z. Liu, R. P. Chang and M. G. Kanatzidis, *J. Am. Chem. Soc.*, 2014*,* **136***,* 16411-16419.
23. Y. Zhao and K. Zhu, *J. Phys. Chem. Lett*., 2013, **4**, 2880−2884.
24. T. Baikie, Y. Fang, J. M. Kadro, M. Schreyer, F. Wei, S. G. Mhaisalkar, M. Gratzel and T. J. White, *J. Mater. Chem. A*, 2013, **1**, 5628−5641.
25. N. Uyeda, T. Kobayashi, K. Ishizuka and Y. Fujiyoshi, *Nature*, 1980, **285**, 95−97.
26. H. Ishii, K. Sugiyama, E. Ito and K. Seki, *Adv. Mater*., 1999, **11,** 605−625.
27. H. Yoshida, K. Inaba and N. Sato, *Appl. Phys. Lett.*, 2007, **91**, 141915.
28. J. H. Lee, Y. Yi and D. W. Moon, *Appl. Phys. Lett.*, 2008, **93**, 153307.
29. L. M. Chen, Z. Xu, Z. Hong and Y. Yang, *J. Mater. Chem.*, 2010, **20**, 2575–2598.
30. Y. Hirose, A. Kahn, V. Arisotov and P. Soukiassian, *Appl. Phys. Lett.,* 1996, **68**, 217.
31. H. Oji, E. Ito, M. Furuta, K. Kajikawa, H. Ishii, Y. Ouchi and K. Seki, *J. Electron Spectrosc. Relat. Phenom.* **1999**, 101–103, 517–521.
32. C. Uhrich, R. Schueppel, A. Petrich, M. Pfeiffer, K. Leo, E. Brier, P. Kilickiran and P. Baeuerle, *Adv. Funct. Mater*., 2007, **17**, 2991–2999.
33. A. Kumar, S. Sista and Y. Yang, *J. Appl. Phys.*, 2009, **105**, 094512.
34. S. T. Lee, Z. Q. Gao and L. S. Hung, *Appl. Phys. Lett*., 1999, **75**, 1404.

35. K. Suemori, M. Yokoyama and M. Hiramoto, *Appl. Phys*., 2006, **99**, 036109.

36. K. Bouzidi, M. Chegaar and A. Bouhemadou, *Sol. Energy Mater. Sol. Cells*, 2007, **91**, 1647–1651.

37. S. Beeby and N. White, (Eds.), *Energy Harvesting for Autonomous Systems*, Artech House, 2010, pp 45-90.

38. M. Bashahu and A. Habyarimana, *Renewable Energy*, 1995, **6**, 127–138.

39. D. Pysch, A. Mette and S. W. Glunz, *Sol. Energy Mater. Sol. Cells*, 2007, **91**, 1698–1706.

40. K. Wang, H. Ren, C. Yi, C. Liu, H. Wang, L. Huang, H. Zhang, A. Karim and X. Gong, *ACS Appl. Mater. Interfaces*, 2013, **5**, 10325–10330.

41. J. H. Son, G. H. Jung and J.-L. Lee, *Appl. Phys. Lett*., 2008, **93**, 012102.

42. K. Sugawara, Y. Minamide, M. Kawamura, Y. Abe and K. Sasaki, *Vacuum*, 2009, **83**, 610–613.

Figure captions

Figure 1 J–V curves for perovskite solar cells with various metal back electrodes.

Figure 2 IPCE spectra of Device PSC-Ag2 and PSC-AgAl, and reflectance spectra of Ag and AgAl layers deposited on FTO slides at a distance of 30 cm.

Figure 3 X-ray diffraction spectra of as-grown porous TiO_2 covered FTO slide (referred as glass/TiO_2) and $CH_3NH_3PbI_{3-x}Cl_x$ deposited on the mesoporous TiO_2 film (referred as glass/TiO_2/$MAPbI_{3-x}Cl_x$).

Figure 4 Cross-sectional elemental analysis of Device PSC-Ag1. Low-resolution TEM micrograph and corresponding elemental maps showing the relative distribution of Ag, Ti, O, Pb, I, Sn and Si.

Figure 5 Cross-sectional high-resolution TEM image of mesoporous TiO_2 film infiltrated with $MAPbI_{3-x}Cl_x$ for Device PSC-Ag1. The cross-section sample was prepared using FIB.

Figure 6 EDX pattern of the AgAl alloy layer deposited at a distance of 30 cm.

Figure 7 Cross-sectional SEM picture of a complete device with an Ag layer deposited at 20 cm. Thick Ag and active layers were prepared for this device.

Figure 8 Cross-sectional SEM images of Ag (a) and AgAl (b) films deposited on HTM-coated FTO slides. The metal layers were thermally evaporated at 30 cm.

Figure 9 Top view SEM images of Ag (a, b) and AgAl (c, d) films deposited on HTM-coated FTO slides. The metal layers were thermally evaporated at 30 cm.

Table 1 Photovoltaic performance of perovskite solar cells with various metal back electrodes.

Table 1

Cell	V_{OC} (V)	J_{sc} (mA cm^{-2})	FF (%)	η (%)	R_{SH} (Ω)	R_S (Ω)
PSC-Ag1	0.84	11.68	56.0	5.49	4753.7	220.7
PSC-Ag2	0.88	15.83	57.9	8.06	4678.2	111.7
PSC-AgAl	0.88	21.11	59.6	11.07	4656.7	81.3

Figure 1

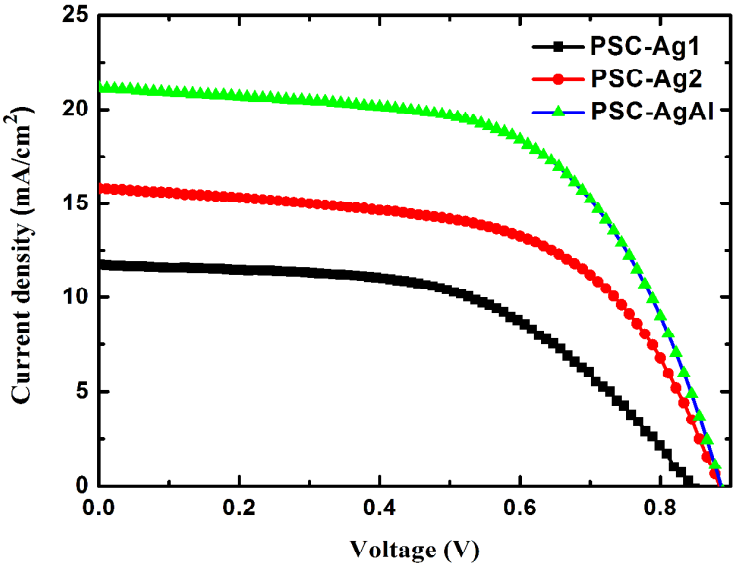

Figure 2

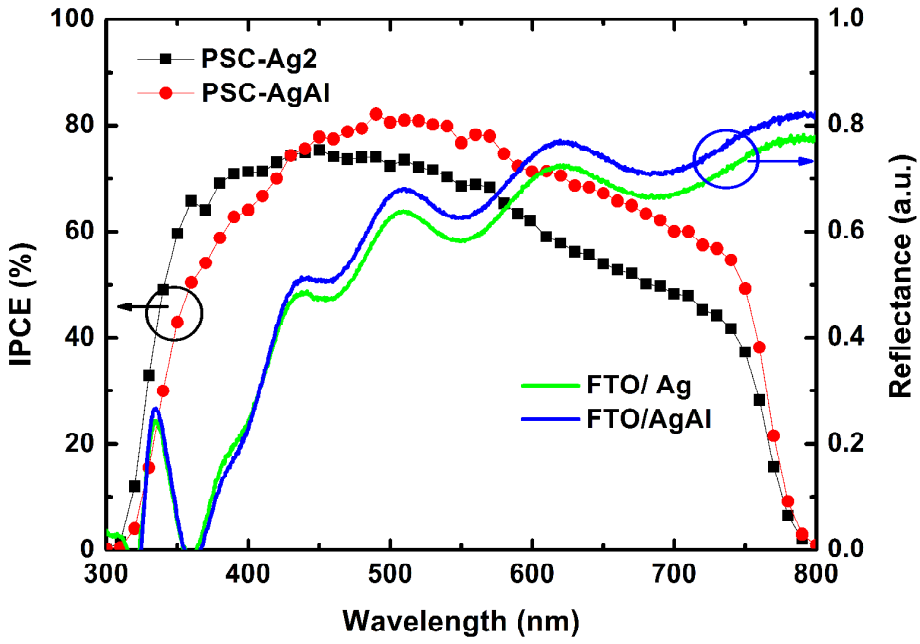

Figure 3

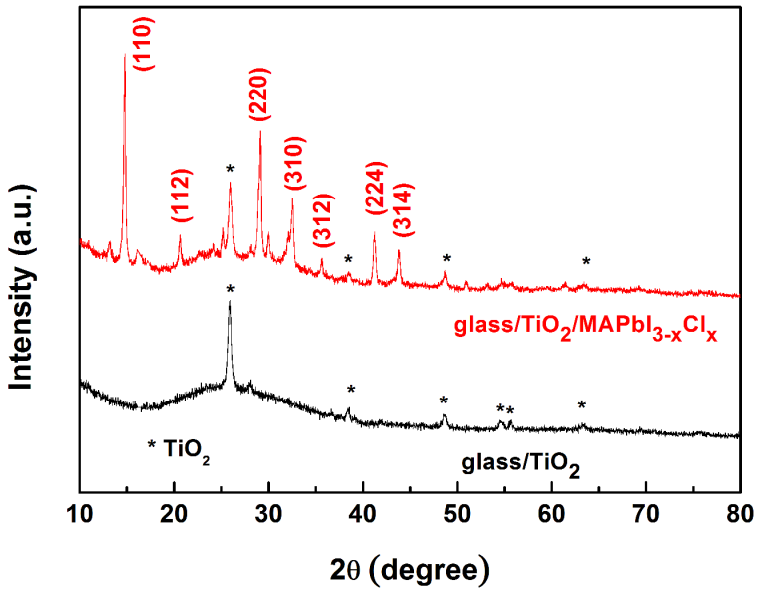

Figure 4

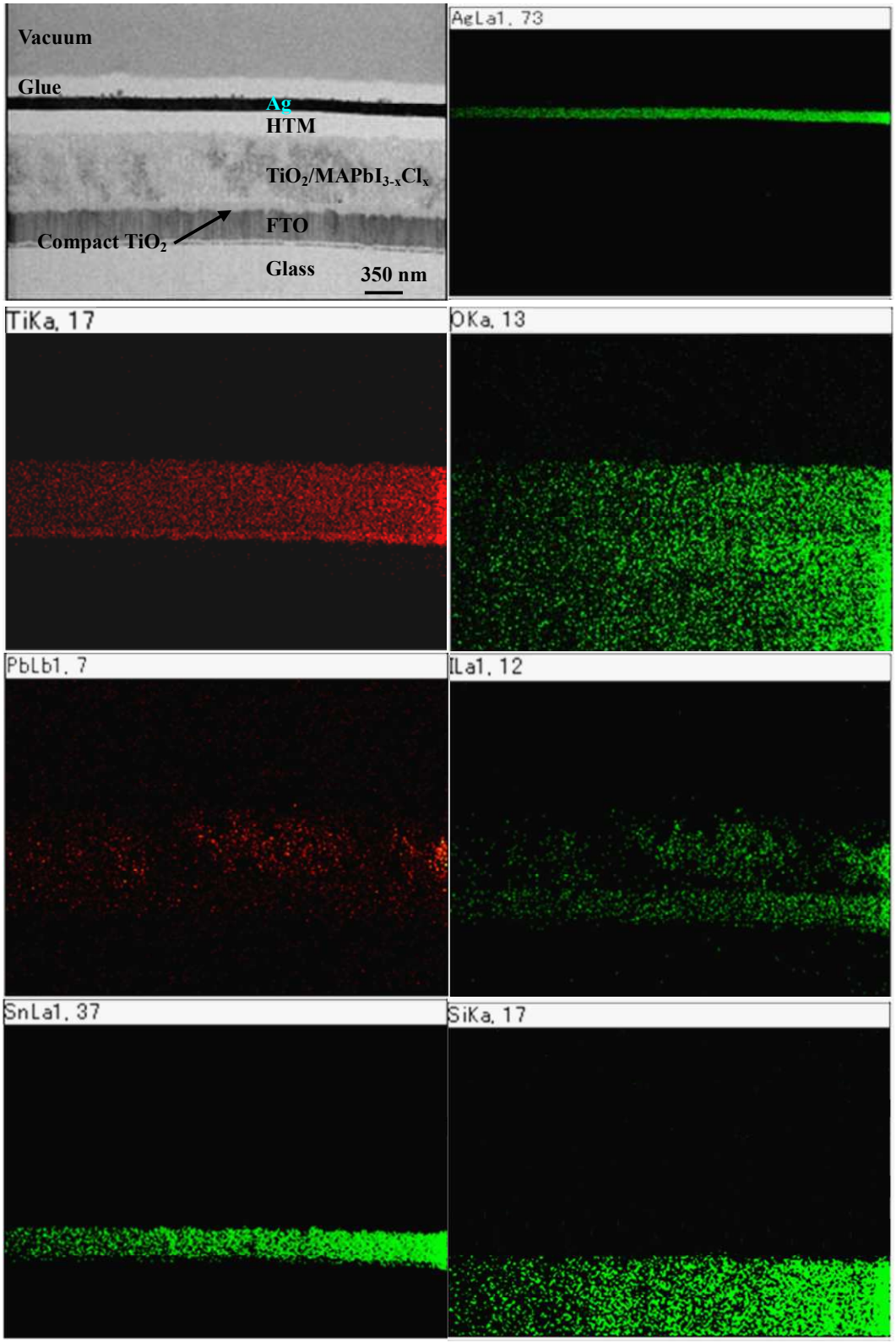

Figure 5 (a)

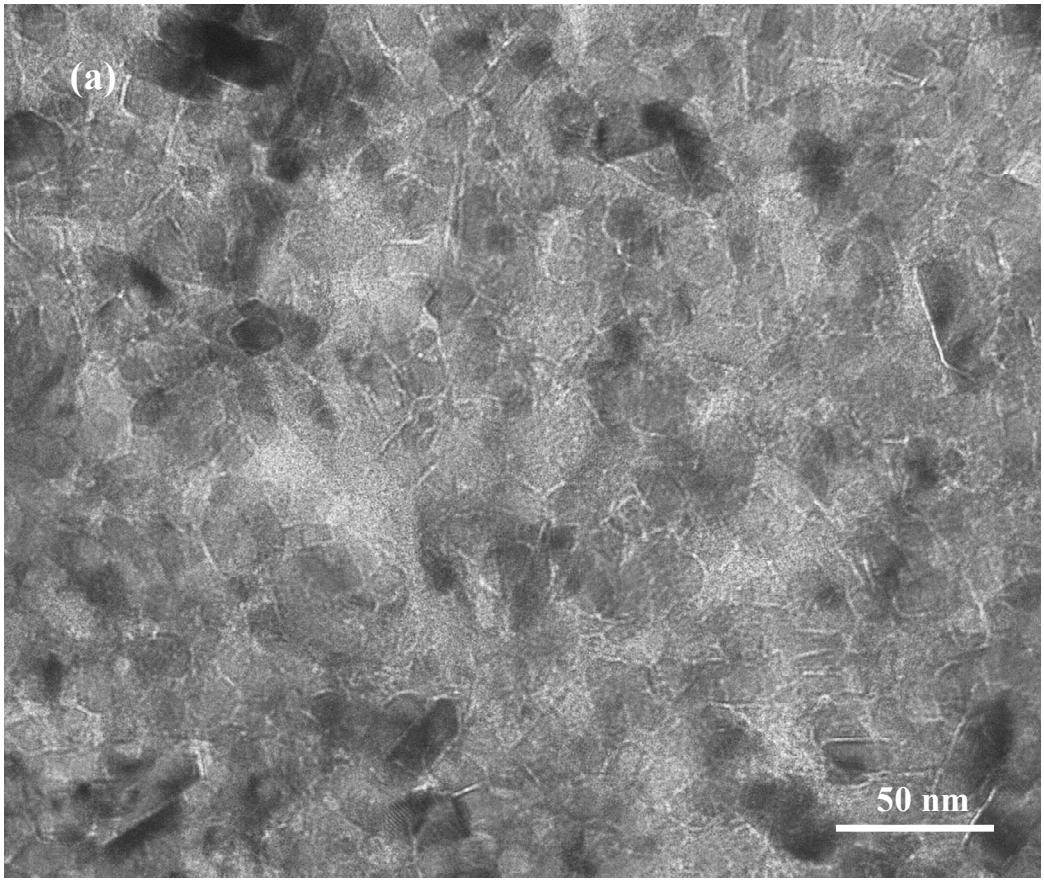

Figure 5 (b)

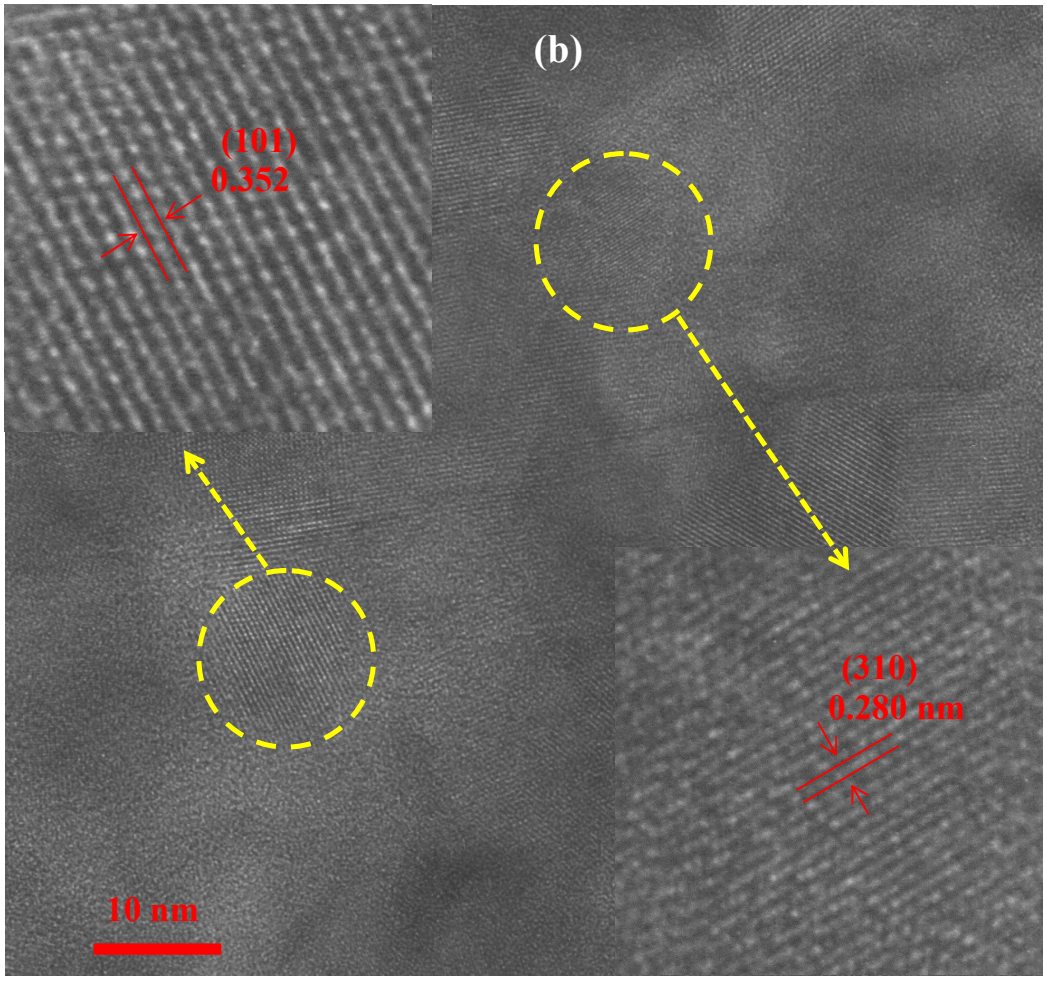

Figure 6

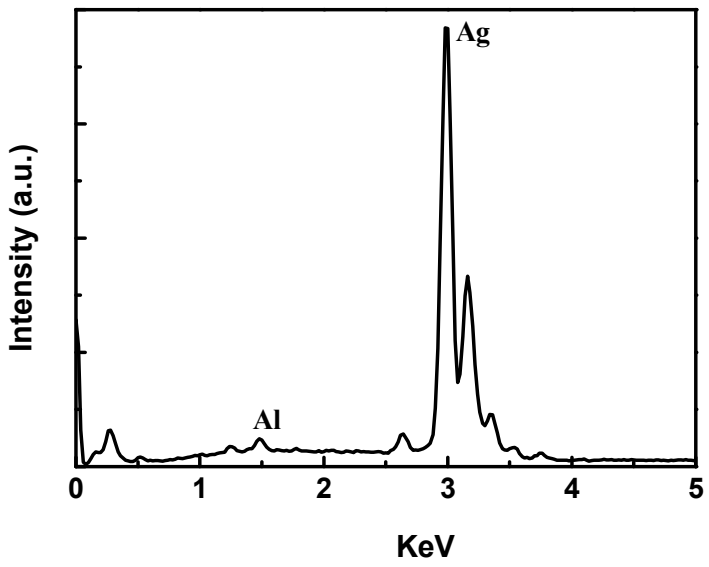

Figure 7

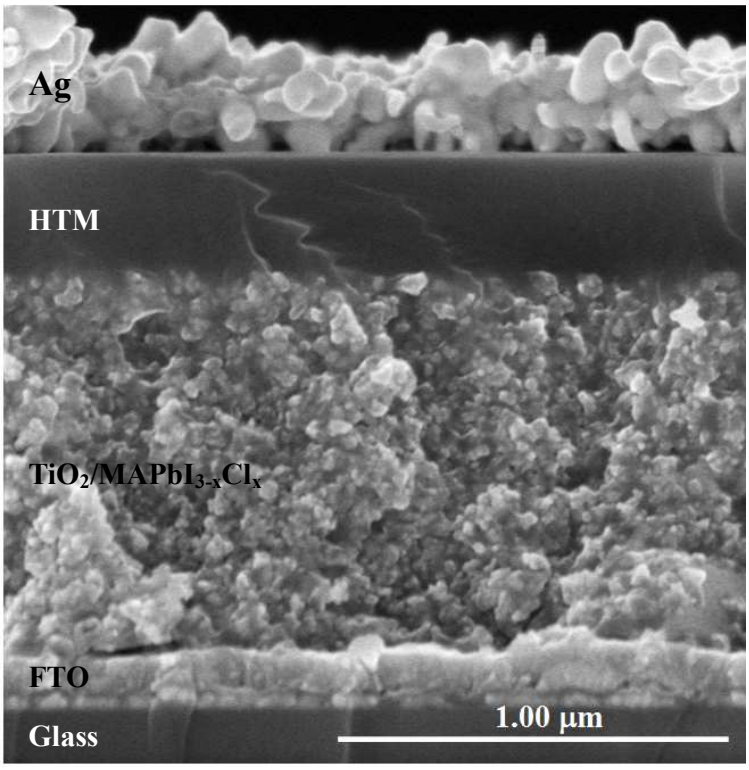

Figure 8 (a)

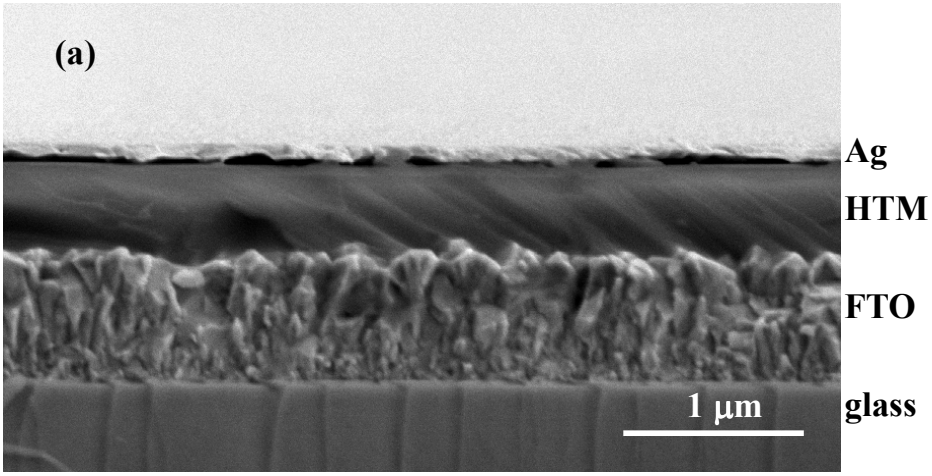

Figure 8 (b)

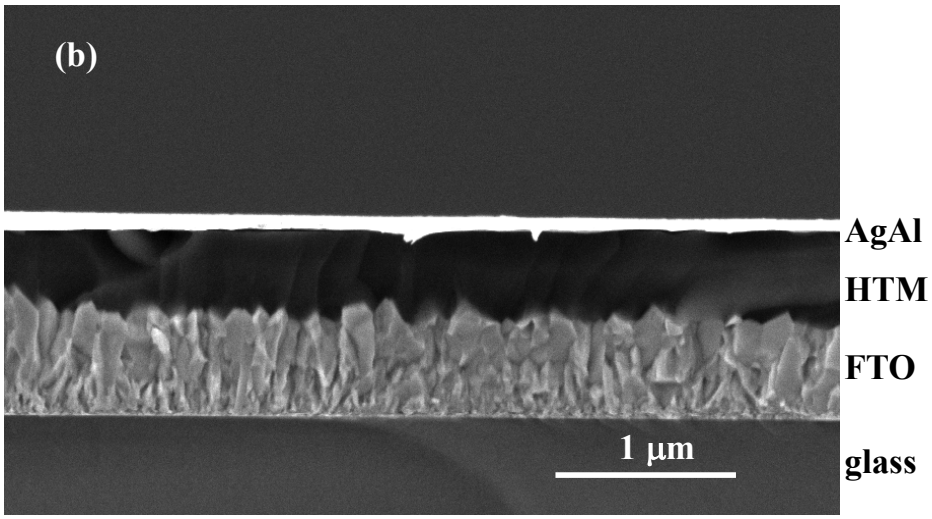

Figure 9 (a)

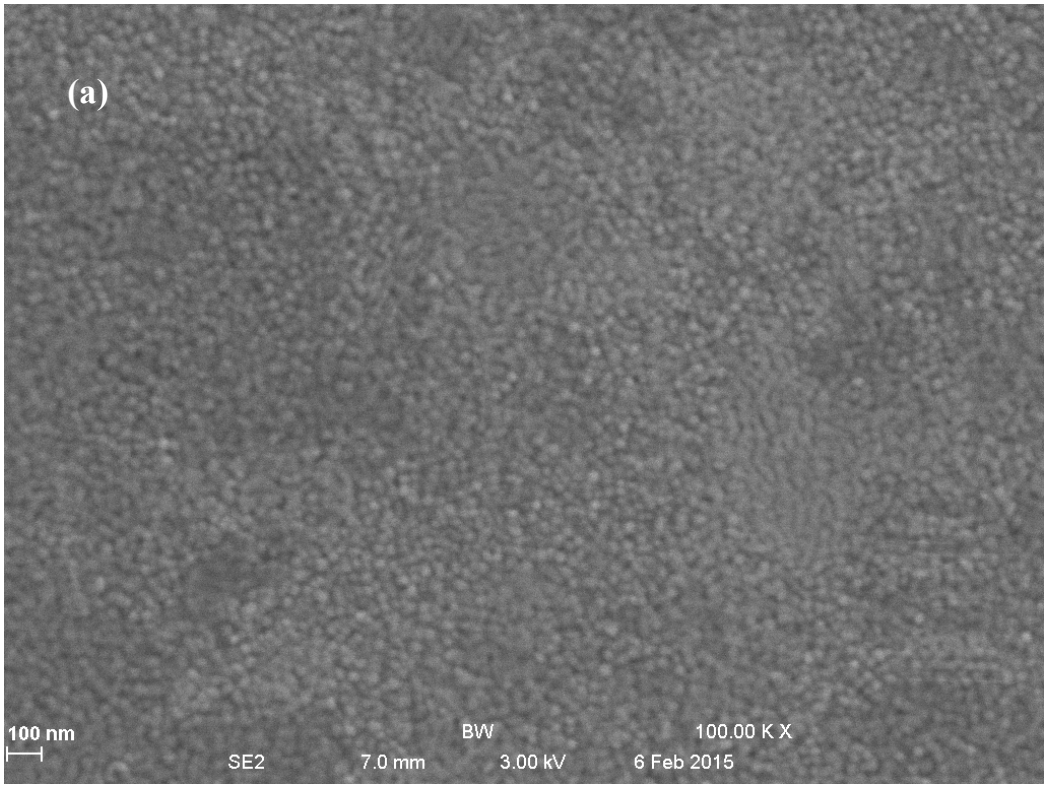

Figure 9 (b)

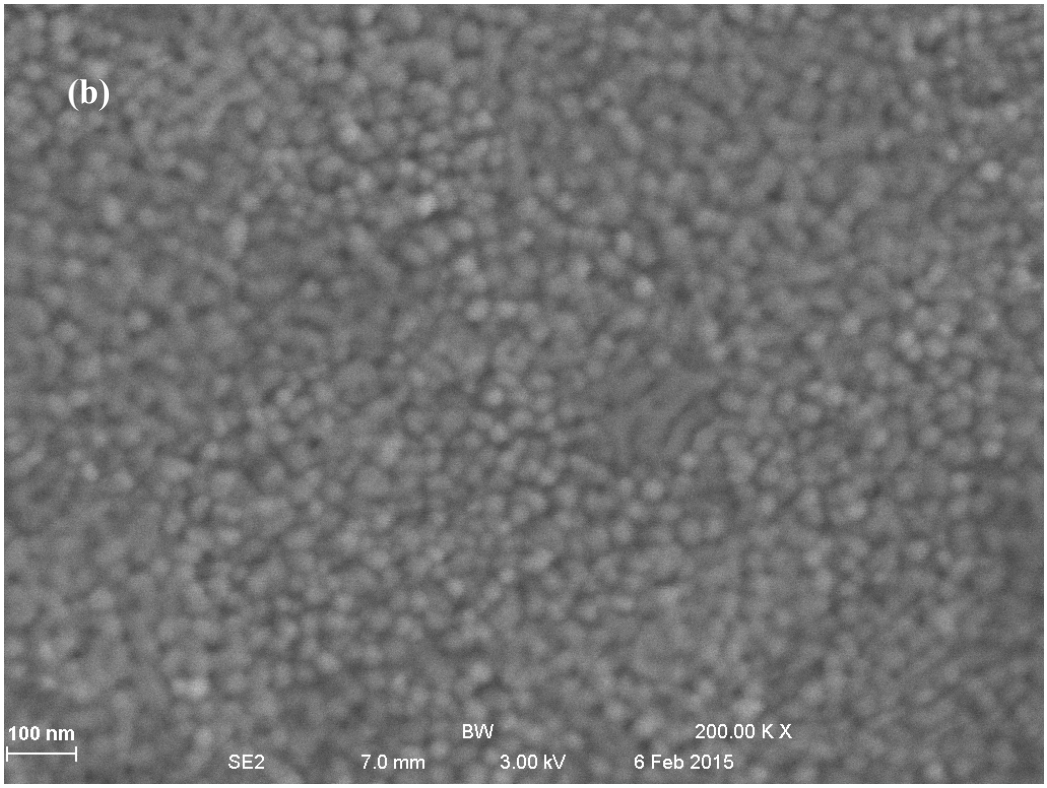

Figure 9 (c)

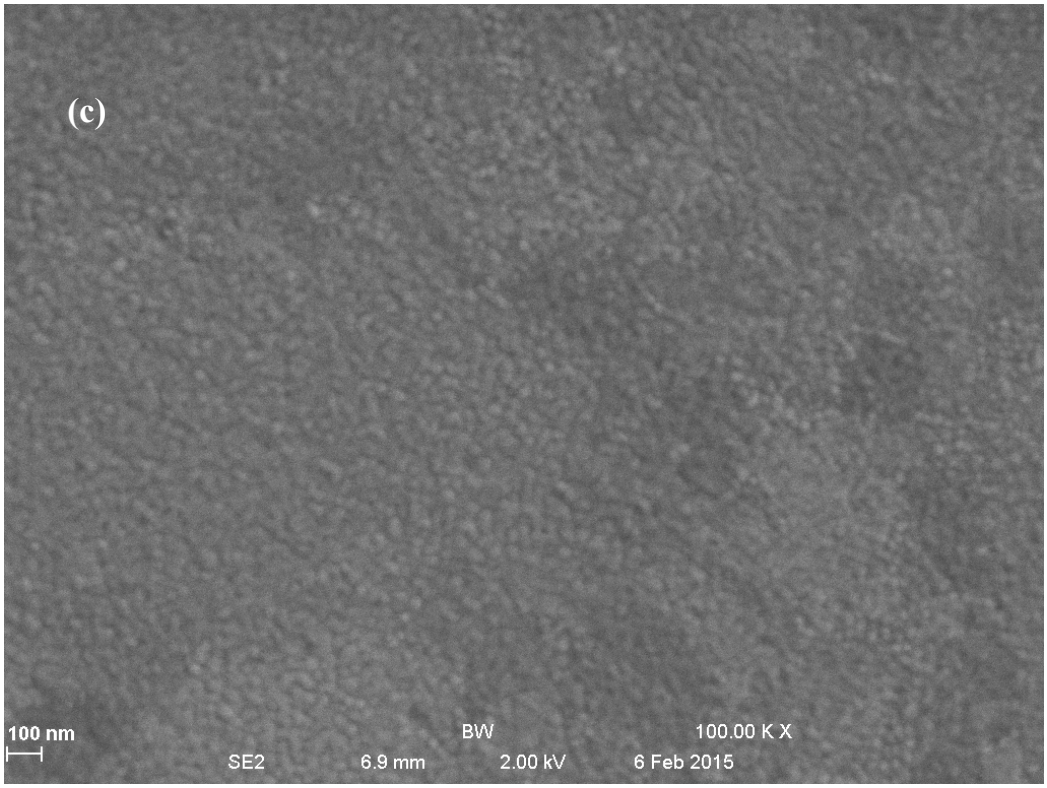

Figure 9 (d)

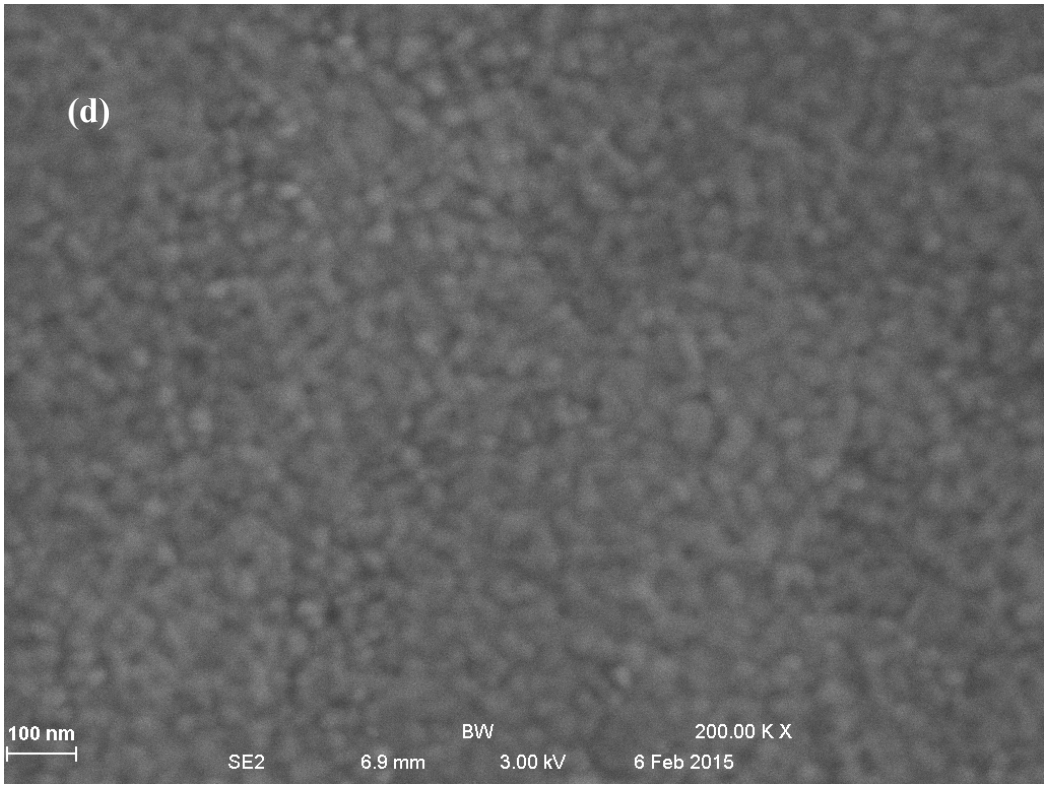

for the Table of contents entry

We demonstrate an efficient mixed halide perovskite solar cell employing thermally evaporated AgAl alloy as a back electrode.